ARMY RESEARCH LABORATORY

Progress in Modeling Ignition in a Solid Propellant Charge for Telescoped Ammunition

by Michael J. Nusca and Albert W. Horst

ARL-TR-3673   **November 2005**

NOTICES

Disclaimers

Army Research Laboratory

Aberdeen Proving Ground, MD 21005-5066

Progress in Modeling Ignition in a Solid Propellant Charge for Telescoped Ammunition

Michael J. Nusca and Albert W. Horst
Weapons and Materials Research Directorate, ARL

REPORT DOCUMENTATION PAGE

1. REPORT DATE *(DD-MM-YYYY)*	2. REPORT TYPE	3. DATES COVERED (From - To)
November 2005	Final	January 2005–May 2005

4. TITLE AND SUBTITLE	5a. CONTRACT NUMBER
Progress in Modeling Ignition in a Solid Propellant Charge for Telescoped Ammunition	
	5b. GRANT NUMBER
	5c. PROGRAM ELEMENT NUMBER
6. AUTHOR(S)	**5d. PROJECT NUMBER**
Michael J. Nusca and Albert W. Horst	622618H8000
	5e. TASK NUMBER
	5f. WORK UNIT NUMBER

7. PERFORMING ORGANIZATION NAME(S) AND ADDRESS(ES)	8. PERFORMING ORGANIZATION REPORT NUMBER
U.S. Army Research Laboratory ATTN: AMSRD-ARL-WM-BD Aberdeen Proving Ground, MD 21005-5066	ARL-TR-3673

9. SPONSORING/MONITORING AGENCY NAME(S) AND ADDRESS(ES)	10. SPONSOR/MONITOR'S ACRONYM(S)
	11. SPONSOR/MONITOR'S REPORT NUMBER(S)

12. DISTRIBUTION/AVAILABILITY STATEMENT

Approved for public release; distribution is unlimited.

13. SUPPLEMENTARY NOTES

14. ABSTRACT

One of the many challenges facing weapon developers is the requirement for a highly lethal, lightweight, and compact large-caliber gun system. A promising concept recently investigated by the U.S. Army is that of a swing-chamber gun, necessitating the use of telescoped ammunition. Such ammunition not only reduces the volume available for the propellant charge, but also places severe geometric constraints on both the distribution of the propellant and the location and functionality of the ignition system. Results of an earlier study highlighted the fact that lumped-parameter interior ballistic codes cannot capture the influence of these configurational complexities on the processes of flamespreading and the ensuing formation of pressure waves. Application of a one-dimensional, two-phase flow code to this problem revealed the likelihood of such waves and raised concern over possible damage to the projectile. Subsequent use of a state-of-the-art, multidimensional interior ballistic code provided quantitative predictions of the flow in the annular region between the sidewall of the telescoped projectile and the cartridge case, detailed the formation of pressure waves, and furthered concern about transient projectile loads. The present report extends this effort, providing results applicable both to comparison with companion gun simulator experiments and appropriate for coupling to projectile/gun structural dynamics codes.

15. SUBJECT TERMS

gun charges, solid propellant, multiphase flow, computer simulation

16. SECURITY CLASSIFICATION OF:			17. LIMITATION OF ABSTRACT	18. NUMBER OF PAGES	19a. NAME OF RESPONSIBLE PERSON
a. REPORT	**b. ABSTRACT**	**c. THIS PAGE**			Michael J. Nusca
UNCLASSIFIED	UNCLASSIFIED	UNCLASSIFIED	UL	32	19b. TELEPHONE NUMBER *(Include area code)* 410-278-6108

Contents

List of Figures

1. Introduction

U.S. Army interest in compact and lightweight future combat systems with maximum capabilities in terms of both lethality and survivability has led to consideration of a number of nonstandard weapon systems and armor approaches. One of the weapon concepts considered has been a compact high-performance, large-caliber gun employing telescoped ammunition as a means of reducing ammunition, and hence overall weapon size and weight. Challenges, in terms of ignition, flamespreading, and attendant pressure-wave formation, as well as overall performance, have motivated efforts at the U.S. Army Research Laboratory (ARL) to model the interior ballistic process for such configurations in increasing detail.

An initial effort (*1*) employed an existing one-dimensional (with area change), two-phase flow interior ballistic code known as XKTC (*2*) to investigated the influence of a nominal, but complex, telescoped ammunition design on flamespreading and pressurization profiles obtained with propellant loaded in either base or base and annular regions of the chamber (see figure 1). A very brief review of results from this preliminary study displays the influence of chamber configuration and charge location on the nature of pressurization within the gun chamber, within the limits of this quasi-one-dimensional representation. Figure 2 presents computational results for an unstructured chamber configuration (lumped-parameter analogy) revealing the expected, well-behaved pressurization at rear (solid line) and forward (dashed line) ends of the chamber. Figure 3 shows the resulting pressure-time curves with propellant loaded only in the region to the rear of the annulus. Figure 4 provides results when propellant is loaded in both rear and annular regions. Figure 3 results were attributed to the change in cross-sectional flow area at the base of the telescoped projectile, leading to rapid increases in local pressures, with subsequent stagnation a flow reversal when the pressure front reached the front boundary of the annulus. This undesirable situation was only exacerbated when propellant was loaded in the annulus as well, the local feedback of locally high pressures into locally high burn rates and hence even higher pressures leading to a rapid over pressurization of the gun chamber, as indicated in figure 4.
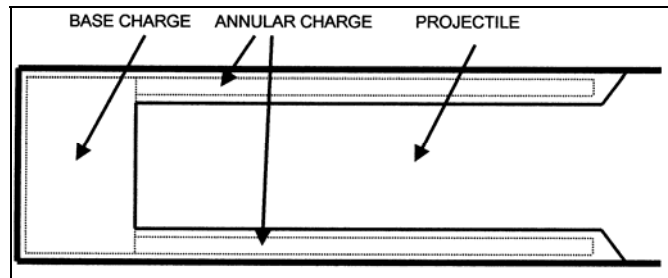
Figure 1. Schematic of simplified telescoped ammunition
configuration (*1*).
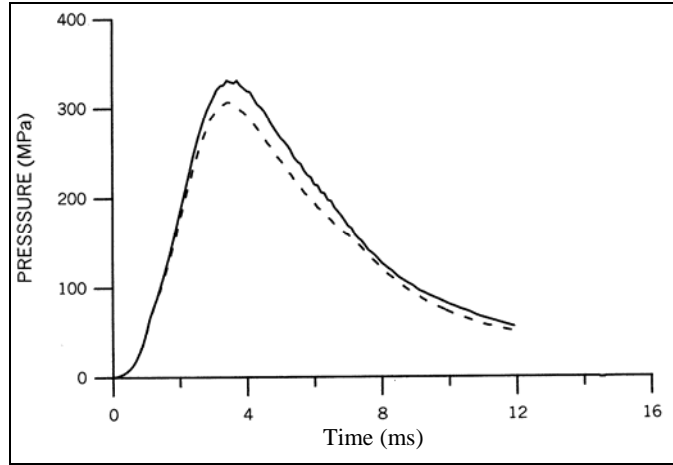
Figure 2. Unstructured chamber (XKTC) (*1*).
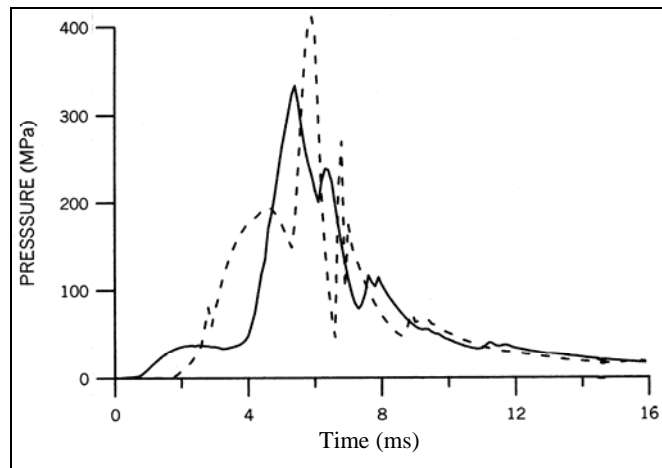
Figure 3. Base charge (XKTC) (*1*).
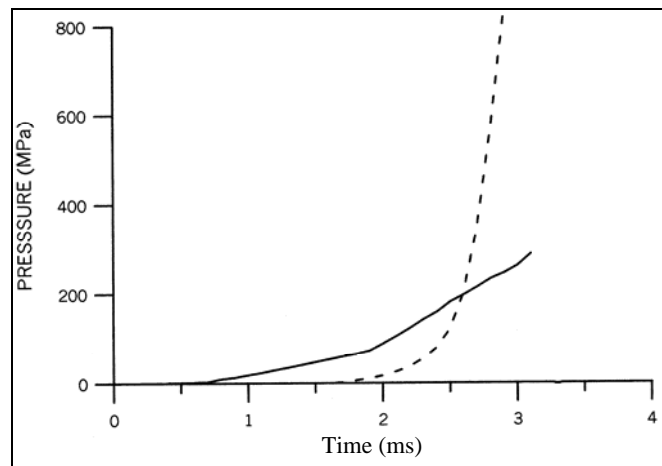
Figure 4. Annular charge (XKTC) (*1*).

A second effort (*3*) extended the analysis though application of the NGEN3 multidimensional, two-phase flow interior ballistic code (*4–6*) to this problem. This code was used to provide a full two-dimensional (2-D), axisymmetric representation of a nominal, degenerate telescoped ammunition configuration (figure 5) with four distinct regions of charge, including two for ignition materials (regions I and II) at the extreme rear of the chamber and two for main charge propellant (region III behind the projectile and region IV in the annular region adjacent to the sidewall of the telescoped portion of the projectile). Figure 6 confirms the prediction of strong longitudinal pressure waves for such a configuration, while figure 7, for the first time, provides details of the pressure fields associated with the development and evolution of these waves. Figure 8 demonstrates a substantial reduction in expected pressure waves accompanying the use of a low drag propellant configuration (concentric wraps) in the annular region.
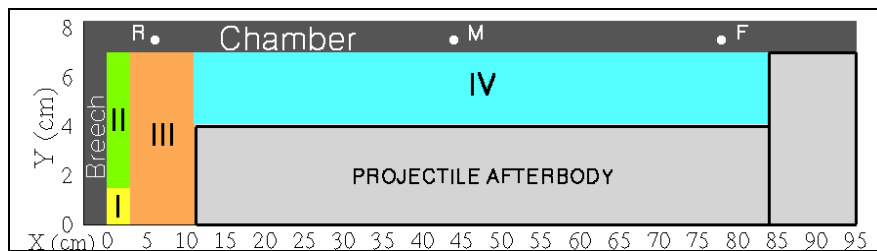
Figure 5. Computational regions (NGEN3) (*3*).
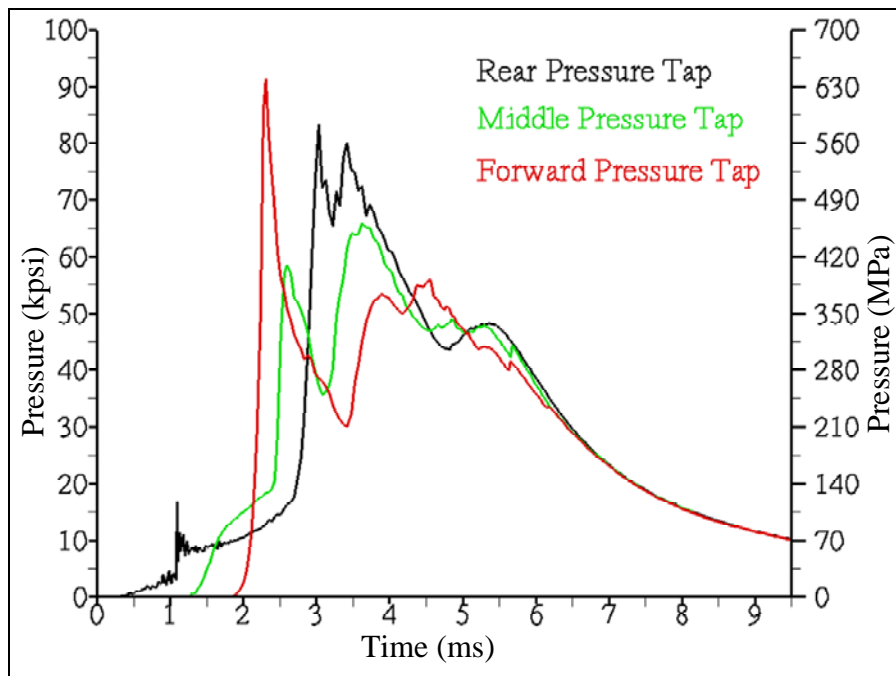
Figure 6. Full charge simulation (NGEN3) (*3*).
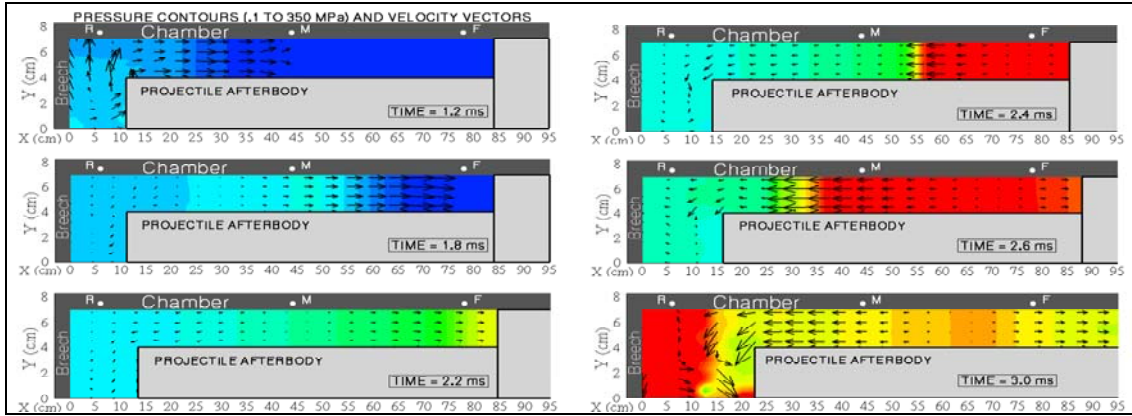
Figure 7. Predicted gas pressure contours (blue to red: 0.1–350 MPa) and velocity vectors for full charge and 1.2–3 ms (NGEN3) (*3*).
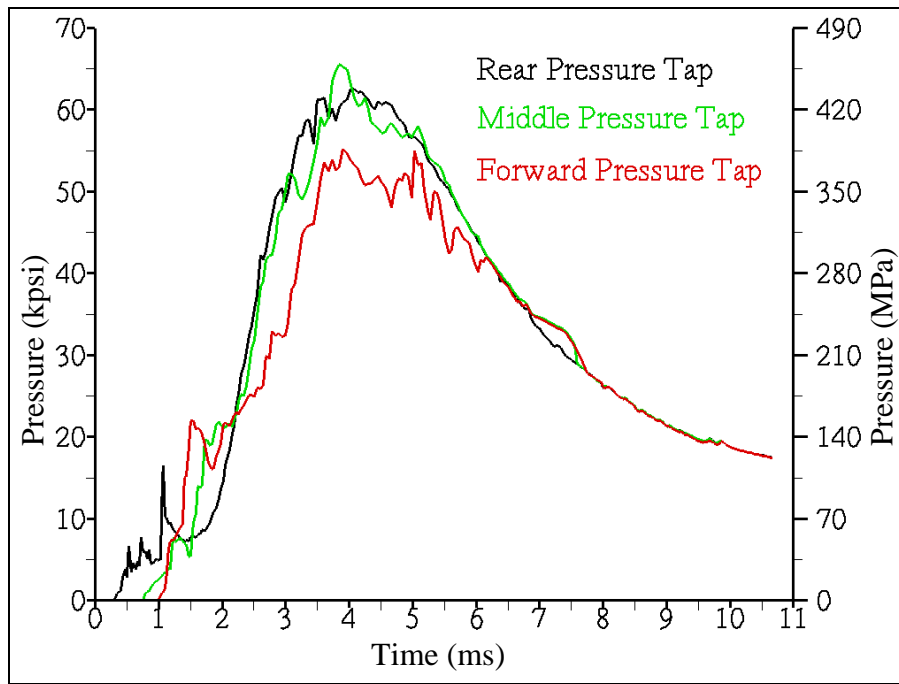
Figure 8. Predicted reduction in pressure waves for full charge of figure 6 with null axial interphase drag in the annular region of propellant (NGEN3) (*8*).

Subsequent studies (*7*, *8*) extended the investigation to probe the impact of such highly dynamic pressure environments on the correspondingly dynamic response of associated projectile structures through the coupling of output from NGEN3 simulations of various telescoped ammunition configurations to Lawrence Livermore National Laboratory's DYNA3D structural mechanics code (*9*) (see figure 9). The negative impact of the presence of strong pressure waves and locally high transient pressures on projectile material stress levels and design requirements was clearly demonstrated, confirming the need to address the design of telescoped ammunition charges and the projectile designs in concert.

4
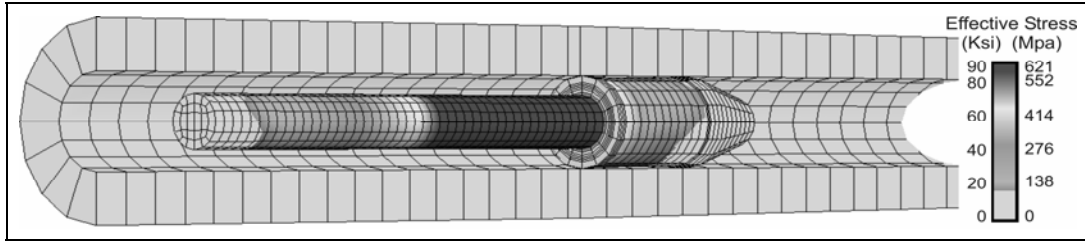
Figure 9. Typical effective stress in projectile wall predicted by DYNA3D using NGEN3 pressure data (*8*).

2.   Current Approach

Recent efforts at ARL have focused on exploitation of coordinated modeling and experimentation efforts to probe charge/projectile interactions associated with the telescoped ammunition configuration. Past efforts employing state-of-the-art interior ballistic codes and plastic-chambered gun chamber simulators (*10–12*) have facilitated the detailed comparison of simulated and measured results, with emphasis on identifying causes and controls for flamespreading anomalies and ensuing deleterious pressure waves in large-caliber guns.

A companion paper (*13*) describes design and initial testing in a large-caliber, telescoped ammunition gun simulator, shown schematically in figure 10 (note locations of strain, S, and pressure, P, gauges). Of specific interest are two test charge configurations, each employing the same ~3-kg charge of 19-perforation, partially-cut JA2 stick propellant, but located in distinctly different portions of the chamber: either all in the base region behind the projectile afterbody or as a shell of propellant filling the annular region adjacent to the wall of the telescoped portion of the projectile and extending to the base of the chamber. Importantly, the projectile has been positioned in the chamber at a location to provide the same propellant loading density (~0.9 g/cm^3) in the regions of the base charge and the shell charge. Ignition is provided by a M123 primer and an accompanying 180-g black powder donut basepad. Moreover, the projectile has been locked in position, focusing the experimental study on flamespreading events prior to projectile motion.
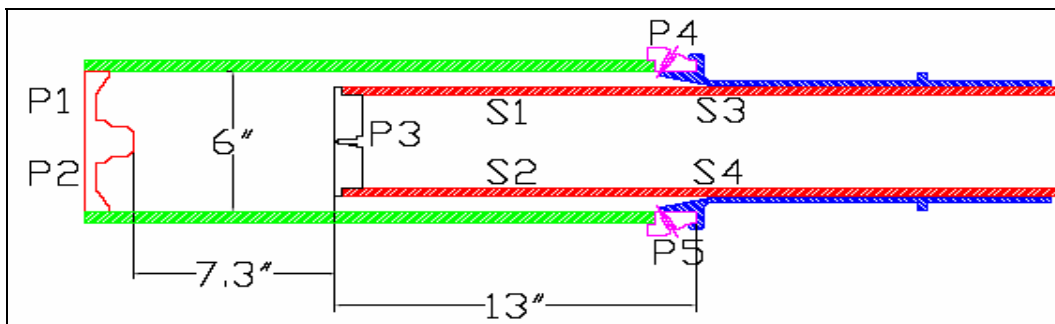
Figure 10. Schematic of simulator used in companion experiments (*13*).

5

In this report, we describe companion calculations from a hierarchy of interior ballistic codes for direct comparison to experimental results obtained using the previously described apparatus, and optionally, to provide additional input for projectile mechanical response studies employing various codes (*14*). The computational study addresses three loading conditions, as displayed in figures 11a–c: rear loading, shell loading, and full chamber. The calculations assume an ~6-l test chamber affixed to a standard 120-mm tank gun barrel, but with a shot start pressure of 21 MPa, sufficient to ensure test chamber failure prior to motion of a 22.3-kg projectile, essentially allowing simulation of both behavior of flamespreading in the test simulator and the full interior ballistic cycle of a nominal 120-mm tank gun.
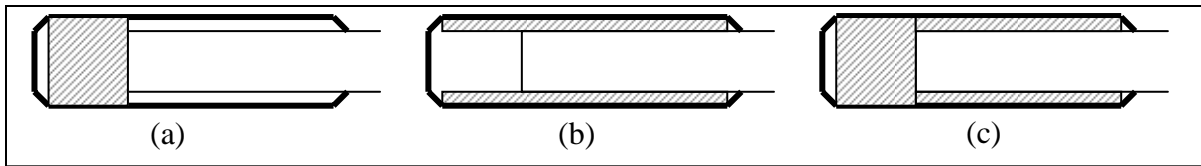
Figure 11. (a) Rear propellant loading; (b) shell propellant loading; and (c) full chamber propellant loading.

Three levels of interior ballistic models are applied to the problem: The IBHVG2 lumped-parameter interior ballistic code; the XKTC one-dimensional (with area change), two-phase flow interior ballistic code; and the NGEN3 multidimensional, two-phase flow interior ballistic code. Briefly, IBHVG2 (*15*) provides a simple but useful lumped-parameter representation of the interior ballistic cycle, embodying such assumptions as uniform and simultaneous ignition of the entire propellant charge, with combustion assumed to take place in a smoothly-varying, well-stirred mixture, the burning rate being determined by the instantaneous, space-mean chamber pressure. An assumed longitudinal pressure gradient is superimposed on the solution at each instant in time to appropriately reduce the pressure on the base of the projectile. An excellent tool for estimating overall performance of a gun, study of ignition-induced pressure waves (a major concern of this study) is clearly outside the physical scope of this model. Furthermore, loading configurations shown in figures 11a and 11b cannot be differentiated in this representation.

Next, the XKTC code (*2*) provides a quasi-one-dimensional, macroscopic (with respect to individual grains), two-phase description of flow in the gun chamber, with the conservation laws formulated to neglect the effects of viscosity and heat conduction in the gas phase. Most importantly, however, gas and solid phases are coupled through heat transfer, combustion, and interphase drag, these processes being modeled using empirical correlations that relate the microphenomena to the average flow properties described by the governing equations. The igniter is either modeled explicitly or treated as a predetermined mass injection profile, and flamespreading follows primarily according to convection, until the ignition temperature is reached and combustion follows at a rate determined by the local pressure. Formulated as a

one-dimensional with area change representation, XKTC provides a first-level capability for treating the dynamics of the axial pressure field and its potential for causing potentially damaging overpressures.

Finally, and of primary interest in the current study, the NGEN3 code (*4–6*) is a multidimensional, multiphase computational fluid dynamics (CFD) code that incorporates three-dimensional continuum equations along with auxiliary relations into a modular code structure. Since accurate charge modeling involves flowfield components of both a continuous and discrete nature, a coupled Eulerian-Lagrangian approach is utilized. On a sufficiently small scale of resolution in both space and time, the components of the flow are represented by the balance equations for a multi-component reacting mixture describing the conservation of mass, momentum, and energy. A macroscopic representation of the flow is adopted using these equations derived by a formal averaging technique applied to the microscopic flow. These equations require a number of constitutive laws for closure including state equations, intergranular stresses, and interphase transfer. The numerical representation of these equations, as well as the numerical solution thereof, is based on a finite-volume discretization and high-order accurate, conservative numerical solution schemes. The spatial values of the dependent variables at each time step are determined by a numerical integration method denoted the continuum flow solver (CFS), which treats the continuous phase and certain of the discrete phases in an Eulerian fashion. The Flux-Corrected Transport scheme (*16*) is a suitable basis for the CFS since the method is explicit and has been shown to adapt easily to massively parallel computer systems. The discrete phases are treated by a Lagrangian formulation, denoted the large particle integrator (LPI), which tracks the particles explicitly and smoothes discontinuities associated with boundaries between propellants yielding a continuous distribution of porosity over the entire domain. The manner of coupling between the CFS and the LPI is through the attribution of properties (e.g., porosity and mass generation) at points in the flow. The size of the grid, as well as the number of Lagrangian particles, is user prescribed. The NGEN3 code takes a macroscopic approach to solid propellant configuration representation. Solid propellant media are modeled using Lagrange particles that regress, produce combustion product gases, and respond to gas-dynamic and physical forces. Individual grains, sticks, slab, and wrap layers are not resolved; rather, each medium is distributed within a specified region in the gun chamber. The constitutive laws that describe interphase drag, form-function, etc., assigned to these various media determine preferred gas flow paths through the media and responses of the media to forces. Media regions can be encased in impermeable boundaries that yield to gas-dynamic flow after a prescribed pressure load is reached.

Application of the NGEN3 code to solid propellant charges for direct-fire weapons of U.S. Army interest is well documented (*3*, *6*, *8*, *17–20*). Clearly, this code is best suited for treatment of the multidimensional aspects of the current problem of interest, and is applied in its latest form to the three charge-loading configurations for the telescoped ammunition chamber simulator described previously.

3. Results of Calculations

3.1   IBHVG2 Simulations

As a lumped-parameter code, input data requirements are essentially limited to gun data (chamber volume, projectile travel, and barrel resistance profile), projectile mass, and energetic material parameters (igniter and main charge masses, dimensions, burning rates, and thermodynamic data). Predicted pressure-time data, provided primarily for reference only, are computed for two loading conditions only (3- and 4.8-kg main charges). The position of the charge in the chamber not being treated by this code, as previously mentioned. The results are presented in figures 12a and 12b, displaying the (necessarily) smooth pressure-time curves with peak pressures of 154 and 435 MPa.
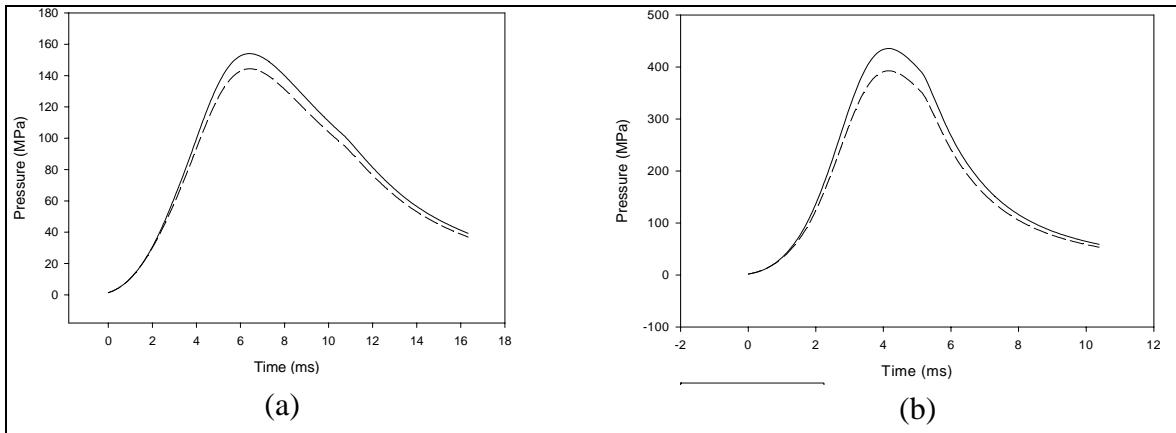
Figure 12. (a) Rear or shell loading (IBHVG2) and (b) full chamber loading (IBHVG2).

3.2   XKTC Simulations

Considerably more interesting are the XKTC results, reflecting the influence of the specific positioning and geometry of propellant charges, projectile, and gun (simulator) chamber, within the one-dimensional-with-area-change approximation. Moreover, these results are influenced by the interphase drag and heat transfer characteristics, as well as bed rheology (i.e., stress fields) associated with the formulation and configuration of the propellant—also beyond the scope of the lumped-parameter representation. Computational problems prevented some of the calculations from going to completion; however, available results for the three configurations are presented in figures 13a–13c. While overall maximum chamber pressures deviate somewhat from the lumped-parameter results, of particular interest are the increasing wave levels as propellant is positioned initially in the confined, annular region adjacent to the projectile, further amplified when the rear region is filled as well. Results for the time and pressure regime of likely interest for comparison to experimental simulator results are enlarged and displayed in figures 14a–14c.
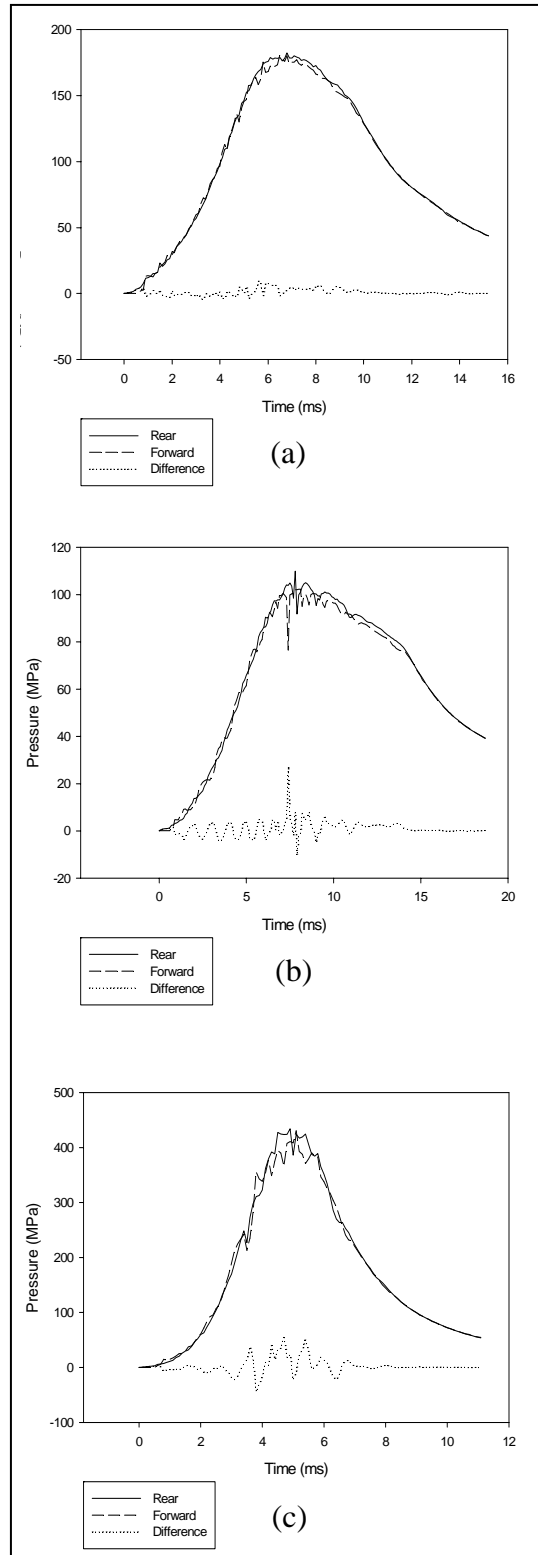
Figure 13. (a) Rear loading (XKTC); (b) shell
            loading (XKTC); and (c) full chamber
            loading (XKTC).

9
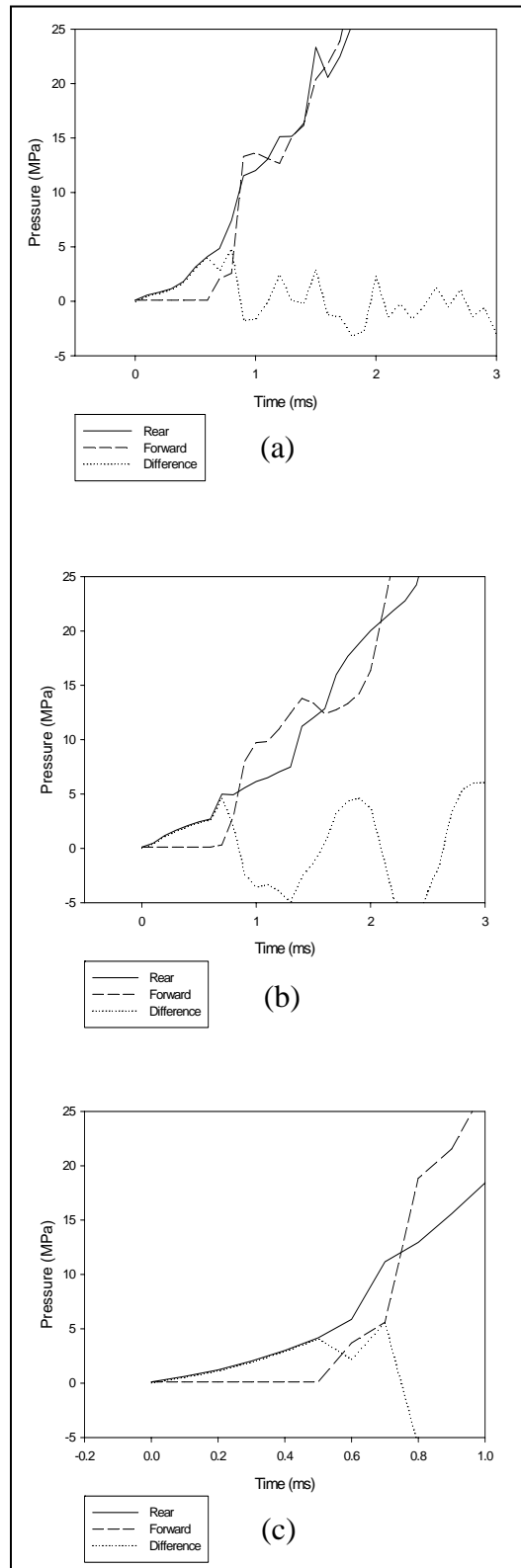
Figure 14. Expanded low pressure regions for
figure 13 data (XKTC).

3.3 NGEN3 Simulations

NGEN3 is the first of the codes applied to the present problem that allows a full 2-D, axisymmetric treatment of the three loading configurations. Further, while the code does not currently support the partially cut multiperforated stick propellant geometry, an excellent approximation can be obtained by using the 19-perforated grain option with the axial interphase drag nulled (actual decrease is indeed about two orders of magnitude). For comparison, calculations were run with both drag levels (i.e., granular and null).

Figure 15 shows the computed pressure/time curves for the three propellant loading configurations, assuming null interphase drag throughout. The plot scales have been chosen to correspond to those used in figures 13. Pressure data was collected at rear, middle, and forward axial stations along the radial wall of the chamber—at 6, 28, and 50 cm from the chamber breech face, respectively. The pressure difference was computed by subtracting the pressure at the forward axial station from that of the rear axial station. Comparing figures 13 and 15, there is a remarkable correspondence between the XKTC-computed and the NGEN3-computed pressure/time curves including the pressure rise rate, the maximum pressure, and the pressure at shot exit. Additionally there is a certain degree of agreement between the two codes as to the wave dynamics in the chamber as evidenced by the oscillations during pressure rise and the pressure differential. Agreement between the codes for results of the amplitude and frequency of pressure differentials is especially remarkable for the case of the shell propellant loading. The NGEN3 code typically demonstrates some degree of pressure fluctuation near the maximum that in part can be contributed to numerical instabilities (*17–20*); in this case, the pressure fluctuations are particularly evident for the full chamber loading (figure 15c). Nevertheless, the degree of agreement between the one-dimensional and 2-D simulations lends credence to both.

Results for the time and pressure regimes of interest for comparison to experimental simulator results are enlarged and displayed in figure 16. Again, the plot scales have been chosen to correspond to those used in figure 14. Here the degree of correspondence between the XKTC and NGEN3 results is less evident. However, certain common patterns can be noted, especially for the shell loading configuration (figures 14b and 16b). Recall that the XKTC code is modeling the solid propellant charge as partially cut multiperforated sticks while the NGEN3 code is using a granular propellant model with null interphase drag. Some of the differences in pressure results for the early stages of flamespreading can be attributed to this difference, especially for the rear loading and the full charge loading configurations (figures 16a and 16c).

The flamespreading process in each propellant loading configuration can be described in greater detail using the NGEN3 code, as demonstrated by the sequence of pressure fields depicting the development and evolution of pressure waves in the chamber (figures 17–19). These series of computed pressure contours, spanning the time from 0.5 to ~5 ms, are shown in color-scale from 0.1 MPa (blue) to the maximum pressure for each time snapshot (red). The plots also contain
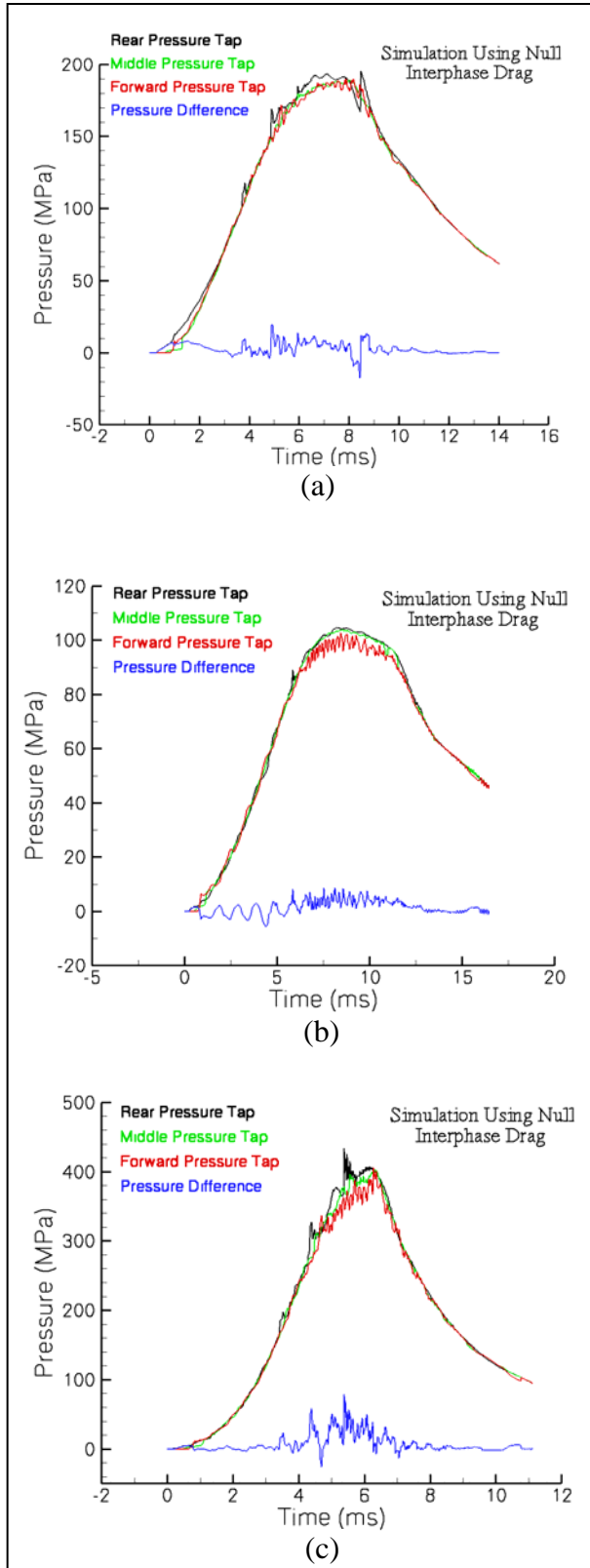
Figure 15. (a) Rear loading (NGEN3); (b) shell loading
(NGEN3); and (c) full chamber loading
(NGEN3).

12
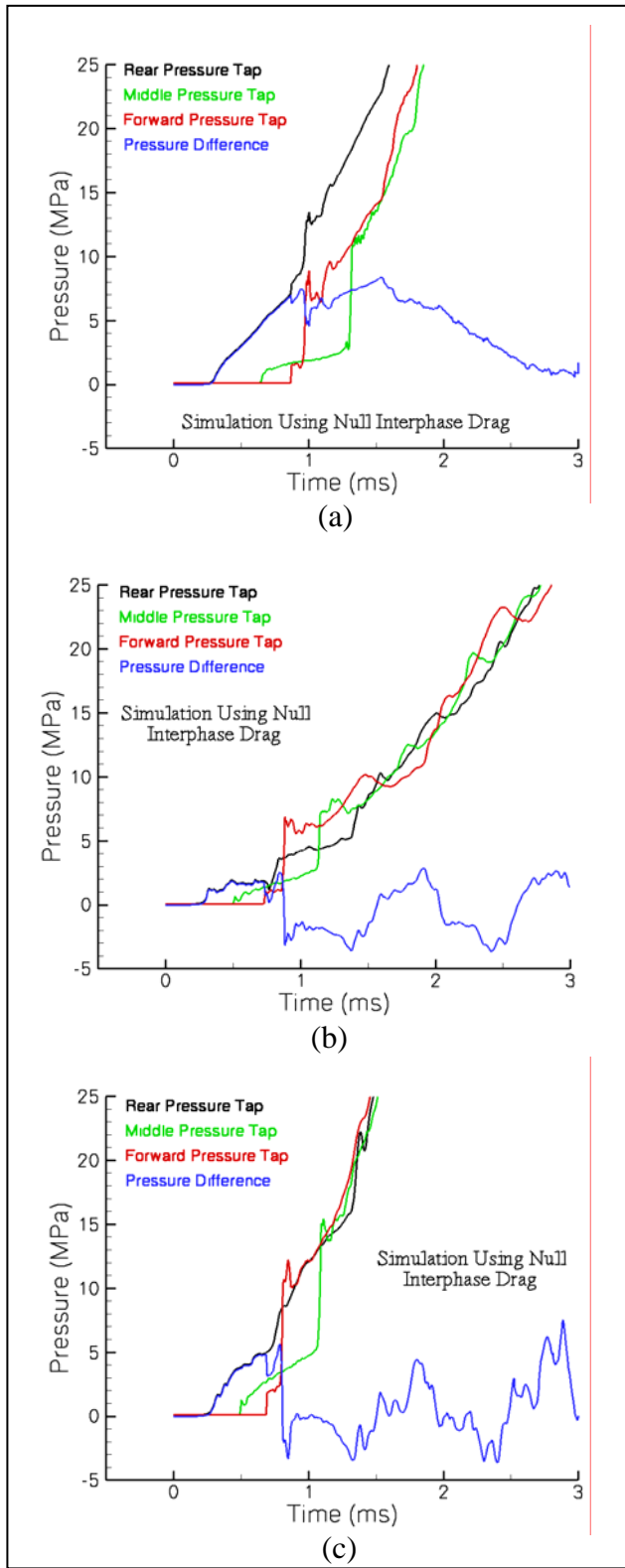
Figure 16. (a) Low pressure region for figure 15a; (b) low pressure region for figure 15b; and (c) low pressure region for figure 15c.

13
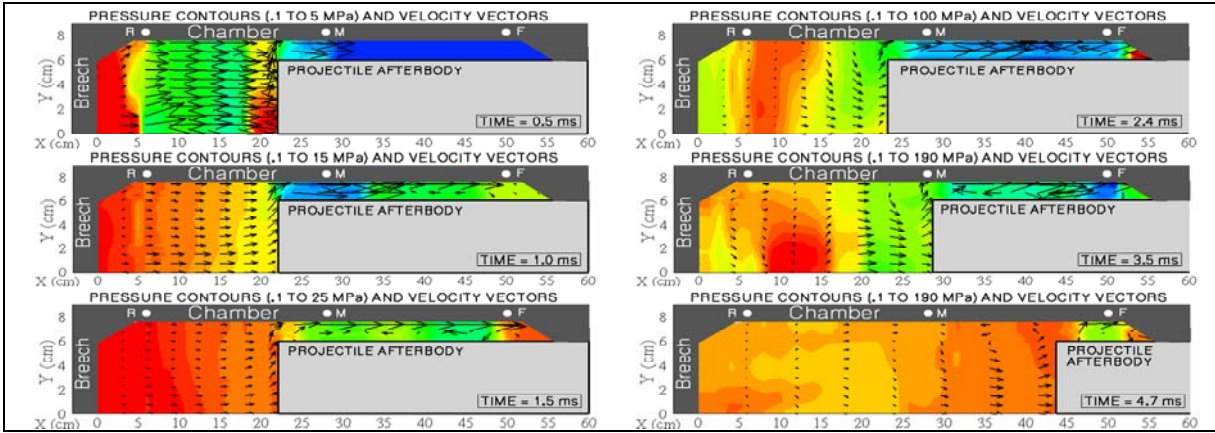
Figure 17. Predicted gas pressure contours (blue to red: minimum to maximum custom scale for each figure) and velocity vectors, rear charge (corresponding to figures 15a and 16a): 0.5–4.7 ms (NGEN3).
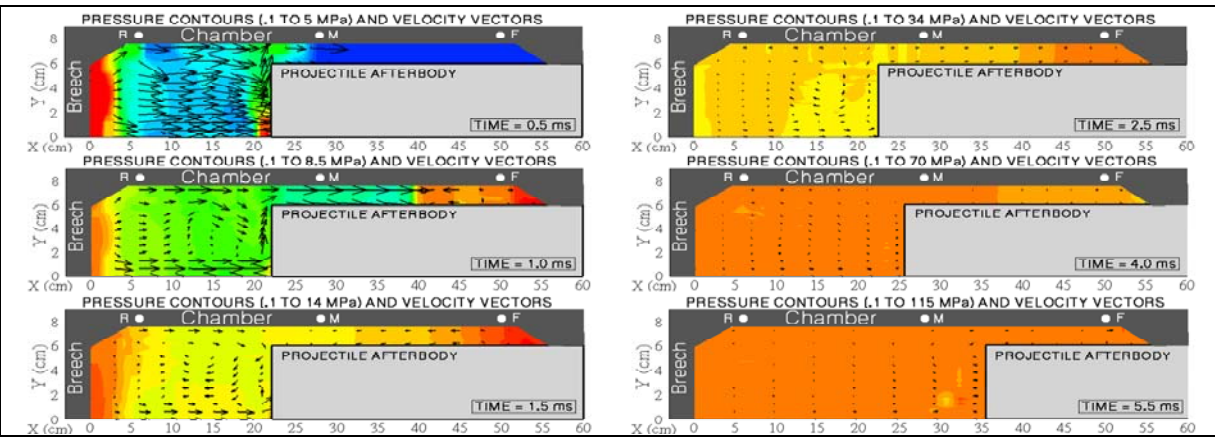
Figure 18. Predicted gas pressure contours (blue to red: minimum to maximum custom scale for each figure) and velocity vectors, shell charge (corresponding to figures 15b and 16b): 0.5–5.5 ms (NGEN3).
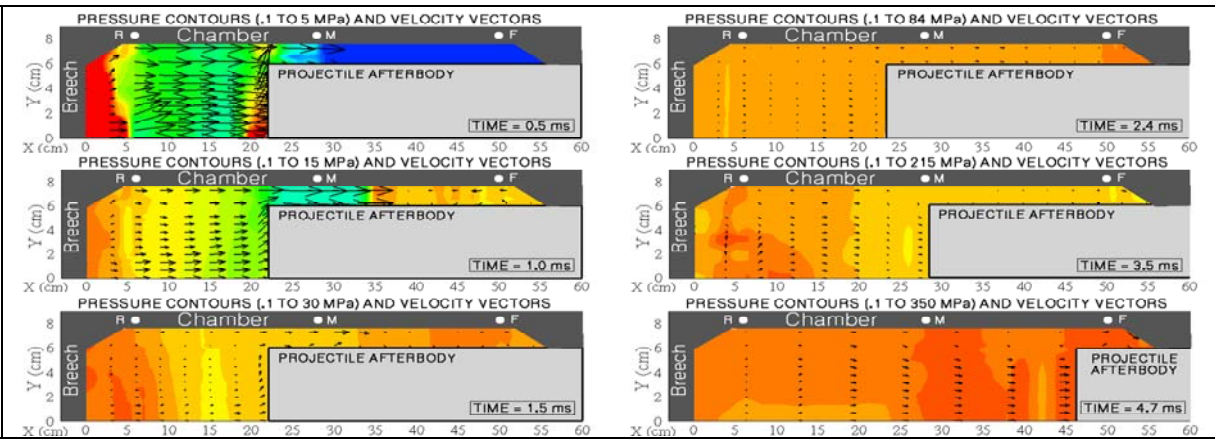
Figure 19. Predicted gas pressure contours (blue to red: minimum to maximum custom scale for each figure) and velocity vectors, full loading (corresponding to figures 15c and 16c): 0.5–4.7 ms (NGEN3).

14

velocity vectors (shown in black) which are overlaid so as to depict both the direction and velocity magnitude of gas movement in the chamber (the scaling for the vectors are the same for all plots). For each time, the chamber and projectile afterbody are shown from the common centerline to the radial wall of the chamber. The locations of the three pressure collection points (R, M, F) used in figures 15 and 16 are also shown along the chamber wall for reference.

The time sequence displayed in figure 17 was computed using the NGEN3 code for the rear loading configuration. High pressure gas is generated along the chamber breech face by the igniter as gas flow is driven forward through the propellant bed located behind the projectile base (0.5 ms). The velocity vectors through this region, between $X = 5$ and 20 cm, are indicative of the low level of interphase drag. Convective heat transfer causes ignition of the propellant and the pressure rises behind the projectile base due to propellant burning and flow stagnation on the base (0.5 ms). Gas flow readily enters the empty annular region from $X = 22$–55 cm, stagnates at the chambrage (1.5 and 3.5 ms) and returns to the rear of the chamber. As the projectile moves (3.5–4.7 ms), flow is drawn into its wake, the propellant bed is completely ignited, and the pressure field is nearly uniform. Consulting figure 16a for this time period, there are no significant negative pressure differentials in the chamber.

The time sequence displayed in figure 18 was computed using the NGEN3 code for the shell loading configuration. High pressure gas is generated along the chamber breech face (0.5 ms) by the igniter as gas flow is driven forward through the propellant bed located along the radial chamber wall (above $Y = 6$ cm) and into the empty region behind the projectile base (below $Y = 6$ cm). The velocity vectors through this annular region are indicative of the low level of interphase drag. Gas flow stagnates on the projectile base and a region of recirculating flow is established in the void behind the base (0.5–1.5 ms). Convective heat transfer causes ignition of the propellant in the annular region around the projectile afterbody as flow stagnation at the chambrage builds pressure in this area and returns flow back toward the breech (1.0 and 2.5 ms). As the projectile moves (4.0–5.5 ms), the propellant bed is completely ignited and the pressure field is nearly uniform. Consulting figure 16b for this time period, there are significant negative pressure differentials generated before projectile movement and a series of pressure waves travel between the chamber breech and forward chambrage.

The time sequence displayed in figure 19 was computed using the NGEN3 code for the full chamber loading configuration. High pressure gas is generated along the chamber breech face by the igniter as gas flow is driven forward through the propellant bed located behind the projectile base and in the annular region around the projectile afterbody (0.5 ms); the velocity vectors through the chamber are indicative of the low level of interphase drag. Convective heat transfer causes ignition of the propellant bed and the pressure rises behind the projectile base due to propellant ignition and flow stagnation on the base (0.5 ms). The propellant in the annular region around the afterbody ignites as flow stagnation at the chambrage builds pressure in this area and returns flow back toward the breech (1.0 and 1.5 ms). The full chamber loading of

propellant is quickly ignited and the pressure field is nearly uniform by 2.4 ms as the projectile is accelerated forward (3.5–4.7 ms). Consulting figure 16c for this time period, there are significant negative pressure differentials between 1.0 and 1.5 ms and around 2.4 ms. The pressure contours displayed below also indicate that the pressure is momentarily higher near the chambrage for certain time periods.

As indicated previously, the NGEN3 code was also run for each of the propellant loading configurations using the granular interphase drag option (figure 20) so that results early in the ballistic cycle (i.e., during ignition and flamespreading) could be compared to the null drag option. With significant interphase drag present, pressurization of the breech is much more rapid for the rear loading and the full chamber loading configurations (comparing figures 16a and 20a as well as figures 16c and 20c). As a result, pressure differentials are always positive as the propellant in the region behind the projectile base ignites promptly. For the shell loading configuration, a comparison of figures 16b and 20b shows that the results are quite similar while the addition of granular drag has the effect of smoothing the pressure curves—retaining the pressure waves while introducing some degree of damping to the ignition event.

4. Conclusions and Future Efforts

As first revealed in our earlier papers (*1*, *3*, *7*, and *8*), the more rigorous studies of the current effort confirm that the telescoped ammunition concept provides a stressful configuration for analysis using even the most sophisticated of interior ballistic codes today. The displacement by a projectile afterbody of chamber volume ordinarily occupied by propellant, and equally significantly, a central ignition system, leads to configurational complexities likely to challenge the real-world charge designer as well as the theoretical interior ballistician. Moreover, the continued requirement for performance will likely require overall propellant loading densities necessitating the presence of propellant in the annular region external to the propellant afterbody. Ignition and combustion in this region complicates not only charge behavior, but also its interface with the adjacent projectile body. The current study has demonstrated the value of the hierarchy of interior ballistic codes in study of this problem: excellent agreement was seen in predicting maximum pressures using all three codes; good agreement was seen in the nature of pressure-wave simulations provided by XKTC and NGEN3; yet only the truly multidimensional representation provided by NGEN3 provided detailed insight into the controlling processes and interactions. Distribution of propellant in the chamber and charge permeability to gas flow during flamespreading and early pressurization, in addition to the projectile/chamber interface itself, are seen to be critical factors in achieving and acceptable interior ballistic environment.
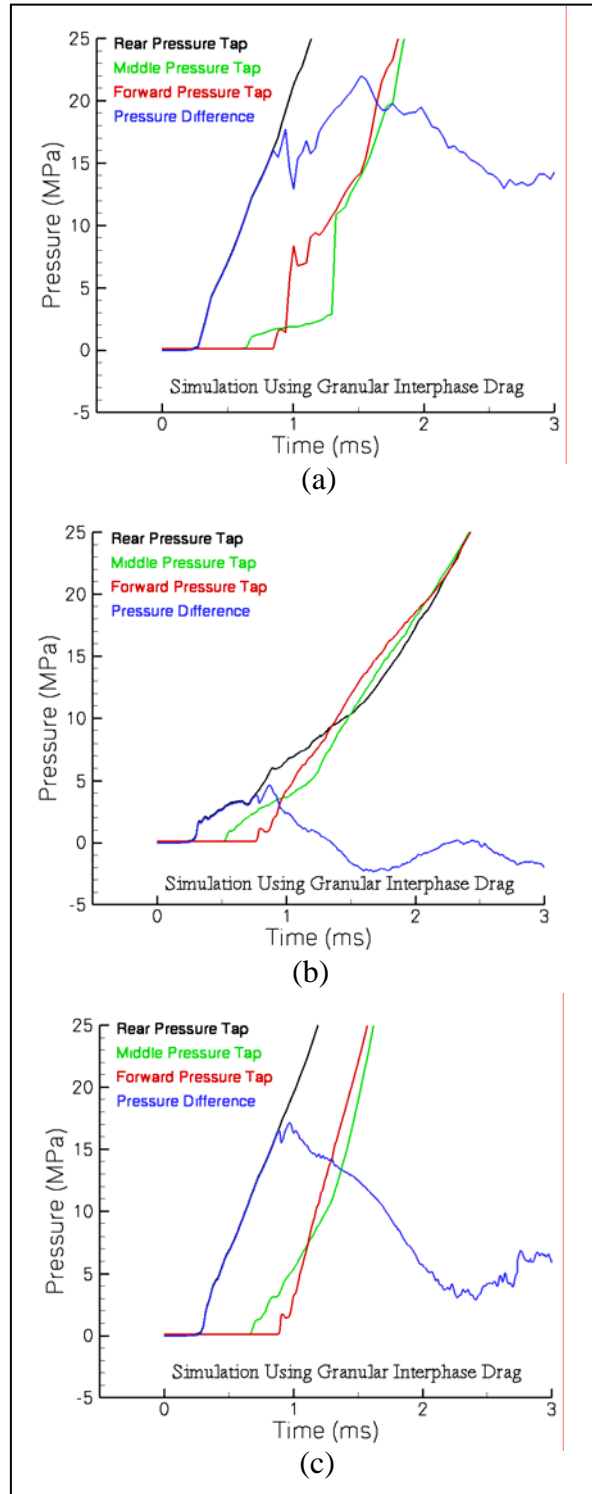
Figure 20. (a–b) Low pressure regions for simulation with granular drag; rear loading (left) and shell loading (right) (NGEN3); and (c) low pressure region for granular drag; full chamber loading (NGEN3).

17

Further value must now be gained from detailed evaluation of our predictive capability against carefully designed ballistic simulator experiments (*13*), allowing comparison of theoretical and experimental parameters not obtainable in the full gun environment. Our aim will then be to provide interior ballistic predictions of ever-increasing fidelity adequate to serve as the detailed loading profiles required to drive the transient projectile response problem (*14*). Clearly, what is needed is a routine and trustworthy approach for coupling an interior ballistic code such as NGEN3 to corresponding numerical codes that model the structural response of the projectile (e.g., DYNA3D and EPIC), so that the overall ammunition designer can arrive at a solution that guarantees the successful launch of a useful payload at a lethal velocity.

5. References

1. Horst, A. W. Weapon System Constraints on Advances in Gun Propulsion, *5th Joint Classified Bombs/Warheads & Ballistics Symposium*, Colorado Springs, CO, 1–2 June 2002.

2. Gough, P. S. *Interior Ballistics Modeling: Extensions to the XKTC Code and Analytical Studies of Pressure Gradient for Lumped Parameter Codes*; ARL-CR-460; U.S. Army Research Laboratory: Aberdeen Proving Ground, MD, February 2001.

3. Nusca, M. J.; Horst, A. W. Progress in Multidimensional, Two-Phase Simulations of Notional Telescoped-Ammunition Solid Propelling Charge. *Proceedings of the 39th JANNAF Combustion Meeting*, CPIA Publication JSC CD-25, December 2003.

4. Gough, P. S. Modeling Arbitrarily Packaged Multi-Increment Solid Propellant Charges of Various Propellant Configurations. *Proceedings of the 33rd JANNAF Combustion Meeting*, CPIA Publication, *653* (*1*), 1996, pp 421–435.

5. Gough, P. S. Extensions to the NGEN Code: Propellant Rheology and Container Properties. *Proceedings of the 34th JANNAF Combustion Meeting*, CPIA Publication, *662* (3), 1997, pp 265–281.

6. Nusca, M. J.; Gough, P. S. *Numerical Model of Multiphase Flows Applied to Solid Propellant Combustion in Gun Systems*, AIAA Paper No. 98-3695, July 1998.

7. Newill, J. F.; Nusca, M. J.; Horst, A. W. Advances in Coupled Projectile-Dynamics/Interior-Ballistics Simulations: Coupling the DYNA3D Code and the ARL-NGEN3 Code. *Proceedings of the 21st International Symposium on Ballistics*, NDIA, Adelaide, South Australia, April 2004.

8. Nusca, M. J.; Horst, A. W.; Newill, J. F. Multidimensional, Two-Phase Simulations of Notional Telescoped-Ammunition Propelling Charge. *Proceedings of the 52nd JANNAF Propulsion Meeting*, CPIA JPM CD-04, May 2004 (see also, U.S. Army Research Laboratory Technical Report ARL-TR-3306, September 2004).

9. Whirley, R. G.; Engelmann, B. E. *DYNA3D – A Nonlinear, Explicit, Three-Dimensional Finite Element Code for Solid and Structure Mechanics*; UCRL-MA-107254 (rev 1); Lawrence Livermore National Laboratory: Oak Ridge, TN, November 1993.

10. Minor, T. C.; Horst, A. W. *Theoretical and Experimental Investigation of Flamespreading Processes in Combustible-Cased Stick Propelling Charges*; BRL-TR-2710; U.S. Army Ballistic Research Laboratory: Aberdeen Proving Ground, MD, February 1986.

11. Nusca, M. J. Numerical Modeling of the Modular Artillery Charge System Using the NGEN Multiphase CFD Code – Effects of case Combustion. *Proceedings of the 37th JANNAF Combustion Subcommittee Meeting*, CPIA Publication, *701* (2), November 2000, pp 87–101.

12. Chang, L.-M.; Howard, S. L.; Hui, P. Y. Experimental Evaluation of Laser-Ignited MACS Increments with a Modified Centercore Ignition System. *Proceedings of the 37th JANNAF Combustion Subcommittee Meeting*, CPIA Publication, *701* (2), November 2000, pp 102–112.

13. Williams, A. et al. Full-scale Simulator Studies of a Notional Telescoped-Ammunition Charge. *Proceedings of the 40th JANNAF Combustion Meeting*, June 2005, in press.

14. Ray, S. E.; Nusca, M. J.; Newill, J. F. A Study of Projectile Response to Ballistics Environment. *Proceedings of the 40th JANNAF Combustion Meeting*, June 2005, in press.

15. Anderson, R.; Fickie, K. *IBHGV2 – A User's Guide*; BRL-TR-2829; U.S. Army Ballistic Research Laboratory: Aberdeen Proving Ground, MD, July 1987.

16. Boris, J. P. et al. *LCPFCT – A Flux-Corrected Transport Algorithm for Solving Generalized Continuity Equations*. NRL-MR/6410-93-7192, April 1993.

17. Nusca, M. J. Application of the NGEN Code to Solid Propellant Charges of Various Propellant Configurations. *Proceedings of the 33rd JANNAF Combustion Meeting*, CPIA Publication, *653*, November 1996, pp 421–435.

18. Nusca, M. J. Application of the NGEN Interior Ballistics Code to High Loading Density and 3-D Propellant Charges. *Proceedings of the 34th JANNAF Combustion Meeting*, CPIA Publication, *662*, October 1997, pp 265–281.

19. Conroy, P. J.; Nusca, M. J. Interior Ballistic Modeling of High-Loading Density Charges in an ETC Gun Using the NGEN Multiphase CFD Code. *Proceedings of the 38th JANNAF Combustion Meeting*, CPIA Publication, *712* (2), April 2002, pp 449–462.

20. Nusca, M. J. Numerical Simulation of Plasma Ignition for High-Loading Density Charges in an ETC Sun Using the NGEN Code. *Proceedings of the 39th JANNAF Combustion Meeting*, CPIA Publication JSC CD-25, December 2003.

NO. OF
COPIES   ORGANIZATION

   1   DEFENSE TECHNICAL
 (PDF   INFORMATION CTR
ONLY)   DTIC OCA
          8725 JOHN J KINGMAN RD
          STE 0944
          FORT BELVOIR VA 22060-6218

   1   US ARMY RSRCH DEV &
          ENGRG CMD
          SYSTEMS OF SYSTEMS
          INTEGRATION
          AMSRD SS T
          6000 6TH ST STE 100
          FORT BELVOIR VA 22060-5608

   1   INST FOR ADVNCD TCHNLGY
          THE UNIV OF TEXAS
          AT AUSTIN
          3925 W BRAKER LN
          AUSTIN TX 78759-5316

   1   DIRECTOR
          US ARMY RESEARCH LAB
          IMNE ALC IMS
          2800 POWDER MILL RD
          ADELPHI MD 20783-1197

   3   DIRECTOR
          US ARMY RESEARCH LAB
          AMSRD ARL CI OK TL
          2800 POWDER MILL RD
          ADELPHI MD 20783-1197

   3   DIRECTOR
          US ARMY RESEARCH LAB
          AMSRD ARL CS IS T
          2800 POWDER MILL RD
          ADELPHI MD 20783-1197

          ABERDEEN PROVING GROUND

   1   DIR USARL
          AMSRD ARL CI OK TP (BLDG 4600)

NO. OF COPIES	ORGANIZATION	NO. OF COPIES	ORGANIZATION
1	DIRECTOR US ARMY RESEARCH LAB AMSRD ARL D J MILLER 2800 POWDER MILL RD ADELPHI MD 20783-1197	18	CDR US ARMY ARDEC D CARLUCCI R CARR R CIRINCIONE S EINSTEIN T GORA J HEDDERICH P HUI
3	DIRECTOR US ARMY RESEARCH LAB AMSRD ARL RO P D MANN R SHAW TECH LIB PO BOX 12211 RESEARCH TRIANGLE PARK NC 27709-2211		J LANNON E LOGSDEN P LU B MACHAK S NICHOLICH P O'REILLY J O'REILLY J RUTKOWSKI A SABASTO J SHIN R SURAPANENI PICATINNY ARSENAL NJ 07806-5000
8	US ARMY AVIATN & MSLE CMD W CHEW C DOLBEER J LILLY M LYON J FISHER B MARSH R MICHAELS D THOMPSON REDSTONE ARSENAL AL 35898-5249	1	COMMANDER RADFORD ARMY AMMO PLANT SMCAR QA HI LIB RADFORD VA 24141-0298
		1	COMMANDER US ARMY NGIC AMXST MC 3 220 SEVENTH ST NE CHARLOTTESVILLE VA 22901-5396
2	PM MAS SFAE AMO MAS M BUTLER PICATINNY ARSENAL NJ 07806-5000	1	COMMANDANT USAFC&S ATSF CN P GROSS FORT SILL OK 73503-5600
2	PM CAS SFAE AMO CAS PICATINNY ARSENAL NJ 07806-5000	2	CDR NAVAL RSRCH LAB TECH LIBRARY J BORIS WASHINGTON DC 20375-5000
7	DIR BENET WEAPONS LAB M AUDINO R DILLON R FISCELLA R HASENBEIN E KATHE K MINER S SOPOK WATERVLIET NY 12189-4050	1	OFFICE OF NAVAL RSRCH J GOLDWASSER 875 N RANDOLPH ST RM 653 ARLINGTON VA 22203-1927

NO. OF COPIES	ORGANIZATION	NO. OF COPIES	ORGANIZATION
8	CDR NSWC J CONSAGA R DOHERTY C GOTZMER S MITCHELL S PETERS T C SMITH C WALSH TECH LIB INDIAN HEAD MD 20640-5000	2	DIR LAWRENCE LIVERMORE NL L FRIED M MURPHY PO BOX 808 LIVERMORE CA 94550-0622
4	CDR NSWC J FRAYSEE R FRANCIS T TSCHIRN TECHLIB DAHLGREN VA 22448-5000	1	CENTRAL INTELLIGENCE AGNCY J BACKOFEN RM 4PO7 NHB WASHINGTON DC 20505
		2	BATTELLE COLUMBUS LAB TWSTIAC V LEVIN 505 KING AVE COLUMBUS OH 43201-2693
3	CDR NSWC A ATWOOD S BLASHILL T PARR CHINA LAKE CA 93555-6001	1	BATTELLE PNL M GARNICH PO BOX 999 RICHLAND WA 99352
1	AIR FORCE RSRCH LAB MNME EN MAT BR B WILSON 2306 PERIMETER RD EGLIN AFB FL 32542-5910	1	BATTELLE EAST SCI & TECH A ELLIS 1204 TECHNOLOGY DR ABERDEEN MD 21001-1228
1	AIR FORCE OFC OF SCI RSRCH M BERMAN 875 N RANDOLPH ST STE 235 RM 3112 ARLINGTON VA 22203-1768	2	JHU CHEM PROP INFO AGNCY W HUFFERD R FRY 10630 LITTLE PATUXENT PKWY STE 202 COLUMBIA MD 21044-3200
1	NASA LANGLEY RSRCH CTR D BUSHNELL MS 110 HAMPTON VA 23681-2199	1	OUSD AT&L/STRAT & TACT SYS MUNITIONS T MELITA 3090 DEFENSE PENTAGON RM 3B1060 WASHINGTON DC 20301-3090
1	DIR SANDIA NATL LAB M BAER DEPT 1512 PO BOX 5800 ALBUQUERQUE NM 87185	1	BRIGHAM YOUNG UNIV M BECKSTEAD DEPT OF CHEMICAL ENGRG PROVO UT 84601
1	DIR SANDIA NATL LAB R CARUNG COMBUSTION RSRCH FACILITY LIVERMORE CA 94551-0469	1	CALIF INSTITUTE OF TECHLGY F CULICK 204 KARMAN LAB MS 301 46 1201 E CALIFORNIA ST PASADENA CA 91109

NO. OF COPIES	ORGANIZATION	NO. OF COPIES	ORGANIZATION
2	UNIV OF ILLINOIS DEPT OF MECH INDUSTRY ENGRNG H KRIER R BEDDINI 144 MEB 1206 N GREEN ST URBANA IL 61801-2978	2	GEN DYNAMICS ORD/TACT SYS N HYLTON J BUZZETT 10101 DR M L KING ST N ST PETERSBURG FL 33716
5	PENNSYLVANIA STATE UNIV DEPT OF MECHANICAL ENGRG K KUO T LITZINGER G SETTLES S THYNELL V YANG UNIV PARK PA 16802-7501	3	GENERAL DYNAMICS ST MARKS J DRUMMOND H RAINES D WORTHINGTON PO BOX 222 ST MARKS FL 32355-0222
1	ARROW TECHLGY ASSOC INC 1233 SHELBURNE RD D 8 SOUTH BURLINGTON VT 05403	1	GENERAL DYNAMICS ARM SYS J TALLEY 128 LAKESIDE AVE BURLINGTON VT 05401
1	ALLEGHENY BALLISTICS LAB PO BOX 210 ROCKET CTR WV 26726	1	HICKS AND ASSOCIATES SAIC I MAY 7990 SCIENCE APPLIC CT VIENNA VA 22182
1	ALLIANT TECHSYSTEMS INC C CANDLAND MN07-LW54 5050 LINCOLN DR EDINA MN 55436	1	PAUL GOUGH ASSOC INC P GOUGH 1048 SOUTH ST PORTSMOUTH NH 03801-5423
3	ATK AMMO & ENERGETICS D WORRELL W WORRELL S RITCHIE RADFORD ARMY AMMO PLANT ROUTE 114 PO BOX 1 RADFORD VA 24141-0299	2	VERITAY TECHGY INC R SALIZONI J BARNES 4845 MILLERSPORT HWY E AMHERST NY 14501-0305
2	ATK THIOKOL P BRAITHWAITE R WARDLE PO BOX 707 BRIGHAM CITY UT 84302-0707	1	SRI INTRNTL PROPULSION SCIENCES DIV TECH LIB 333 RAVENWOOD AVE MENLO PARK CA 94025-3493
1	ATK ELKTON J HARTWELL PO BOX 241 ELKTON MD 21921-0241	1	SAIC W WAESCHE 1410 SPRING HILL RD ST 400 MCLEAN VA 22102
1	BAE ARMAMENT SYS DIV J DYVIK 4800 E RIVER RD MINNEAPOLIS MN 55421-1498	2	ATK TACTICAL SYS T FARABAUGH W WALKUP PO BOX 707 BRIGHAM CITY UT 84302-0707

ABERDEEN PROVING GROUND

1	CDR USA ATC
	STECS LI
	R HENDRICKSEN
	APG MD 21005
45	DIR USARL
	AMSRD ARL WM
	W CIEPIELA
	D LYON
	AMSRD ARL WM B
	J MORRIS
	M ZOLTOSKI
	AMSRD ARL WM BA
	T KOGLER
	AMSRD ARL WM BC
	P PLOSTINS
	AMSRD ARL WM BD
	W ANDERSON
	R BEYER
	A BRANT
	S BUNTE
	T COFFEE
	J COLBURN
	P CONROY
	N ELDREDGE
	B FORCH
	B HOMAN
	A HORST
	S HOWARD
	P KASTE
	A KOTLAR
	C LEVERITT
	R LIEB
	K MCNESBY
	M MCQUAID
	M MILLER
	A MIZIOLEK
	J NEWBERRY
	M NUSCA (6 CPS)
	R PESCE-RODRIGUEZ
	G REEVES
	B RICE
	R SAUSA
	E SCHMIDT
	A WILLIAMS
	AMSRD ARL WM BF
	D WILKERSON
	AMSRD ARL WM EG
	J SCHMIDT
	AMSRD ARL WM M
	S MCKNIGHT

NO. OF COPIES	ORGANIZATION
	AMSRD ARL WM SG
	T ROSENBERGER
	AMSRD ARL WM T
	B BURNS
	ARSRD ARL WM TB
	P BAKER

INTENTIONALLY LEFT BLANK.